Journal of Power Sources, 22 (1988) 323 - 340

EXAFS: A NEW TOOL FOR THE STUDY OF BATTERY AND FUEL CELL MATERIALS

JAMES McBREEN and WILLIAM E. O'GRADY

Brookhaven National Laboratory, Department of Applied Science, Upton, NY 11973 (U.S.A.)

KAUMUDI I. PANDYA

Case Western Reserve University, Physics Department, Cleveland, OH 44106 (U.S.A.)

Summary

Extended X-ray absorption fine structure (EXAFS) is a powerful technique for probing the atomic structure of battery and fuel cell materials. The major advantages of EXAFS are that both the probe and the signal are X-rays and the technique is element-selective and applicable to all states of matter. This permits *in situ* studies of electrodes and determination of the structure of single components in composite electrodes or even complete cells. EXAFS specifically probes short range order and yields coordination numbers, bond distances, and chemical identity of nearest neighbors. Thus, it is ideal for structural studies of ions in solution and the poorly crystallized materials that are often the active materials or catalysts in batteries and fuel cells. This paper uses studies on typical battery and fuel cell components to describe the technique and the capability of EXAFS as a structural tool in these applications. Typical experimental and data analysis procedures are outlined. The advantages and limitations of the technique are discussed. Other techniques using high intensity synchrotron X-rays are also briefly discussed.

Introduction

The performance and life of batteries and fuel cells are often determined by subtle aspects of the structure of various components. Examples of these inter-relationships are as follows:

(i) lead–acid battery life is determined by the structure of the basic lead sulfates in the cured plates [1];

(ii) zinc–manganese dioxide battery performance strongly depends on the structure of MnO_2 [2];

(iii) swelling of nickel electrodes is related to the structure of $Ni(OH)_2$ [3];

(iv) the activity and stability of carbon supported platinum catalysts are dependent on strong carbon platinum interactions [4];

0378-7753/88/$3.50

(v) the quality of zinc deposits in flow batteries [5] and the efficiency of redox systems are related to electrolyte structure [6, 7].

Structural determinations of battery and fuel cell electrode materials are often very difficult. The situation is exacerbated when *in situ* determinations are attempted. Often these materials are amorphous and exhibit very weak, or even no, X-ray diffraction patterns. Examples are $Ni(OH)_2$, NiOOH [8], MnO_2 [9], and pyrolyzed metal–macrocyclic electrocatalysts [10]. Many battery materials such as NiOOH and the discharge products of MnO_2 are hydrated, so meaningful *ex situ* measurements using various photoelectron spectroscopies are nearly impossible. Some *in situ* methods are of limited value because they require specular surfaces (reflectance spectroscopy and ellipsometry) or are applicable only to a few elements (Mössbauer spectroscopy and SERS (surface enhanced Raman spectroscopy)). Interpretation of spectroscopic data (*e.g.*, Raman spectroscopy or photoacoustic spectroscopy (PAS)) from a typical electrode containing additives, conductive diluents, electrolyte, and plastic binders is essentially impossible.

Determination of the structure of electrolytes is also a problem. The application of various scattering (*e.g.*, Raman) and absorption (*e.g.*, infrared and nuclear magnetic resonance (NMR)) spectroscopies to electrolyte studies has been critically reviewed [11]. In many cases the lack of a reliable theoretical framework has led to conclusions that are qualitative in character. This is particularly true when the spectroscopies are applied to hydrated ions. For instance, the Raman method is not able to yield information about ion–water distances in solution. In the case of neutron scattering, even in concentrated solutions, ion–water contributions to the total scattering pattern are only about 10%. This makes elucidation of the ion–water terms very difficult.

The present paper discusses how EXAFS can help in these structural determinations. The basic principles, the experimental methods, and data analysis for EXAFS will be outlined. This will be done using examples of EXAFS studies on typical battery and fuel cell components.

The EXAFS technique

Experimental aspects

An EXAFS experiment is simply the accurate determination of the X-ray absorption coefficient (μ) of a material, as a function of photon energy, in an energy range that is below and above an absorption edge of one of the elements in the material. The most direct method is to do a transmission X-ray absorption experiment. Figure 1 is a schematic representation of the experimental configuration. It consists of an X-ray source, a double-crystal monochromator, a thin sample of the material, detectors for monitoring the X-ray beam before, and after, it passes through the material, and a data acquisition system. The data acquisition system is used for several purposes. This includes stepping the monochromator to pass the desired

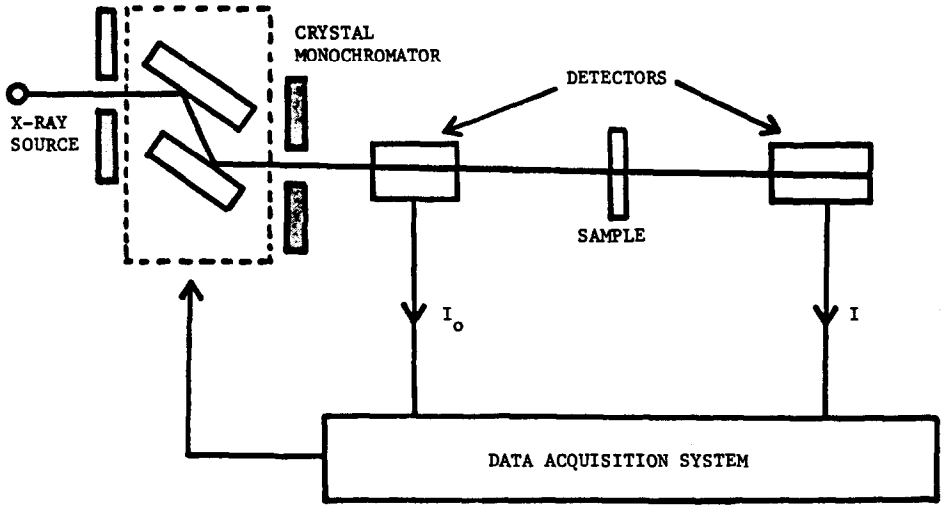

Fig. 1. Experimental setup for transmission EXAFS measurements.

photon energies (E), alignment of the sample in the beam, and monitoring the signals from the detectors.

The origin of EXAFS

EXAFS is the result of a photoelectric absorption process. In most cases X-ray absorption involves the interaction of X-rays with the outer shell electrons of elements. This can be described by the simple Lambert equation

$$I = I_0 \exp(-\mu x) \tag{1}$$

where I_0 is the intensity of the incident photon beam, I the intensity of the transmitted beam, and x the thickness of the sample. Figure 2 is an X-ray absorption spectrum for a dry, plastic-bonded, nickel oxide electrode. The initial monotonically decreasing part of the curve, where μ is approximately proportional to E^{-3}, can be described by eqn. (1) and is determined by the chemical composition of the electrode, including all the elements in the conductive diluent, the $Co(OH)_2$ additive, and the plastic binder. When the X-ray energy (8337 eV) is sufficient to liberate an inner nickel K-shell electron, and excite it to an unoccupied continuum state, an abrupt increase in the absorption is observed. This is called the absorption edge and is unique to the element. For photon energies greater than E_b = 8337 eV, the ejected photoelectron travels as an outgoing spherical wave with a wavelength (λ)

$$\lambda = \frac{2\pi}{k} \tag{2}$$

where k, the photoelectron wave vector,

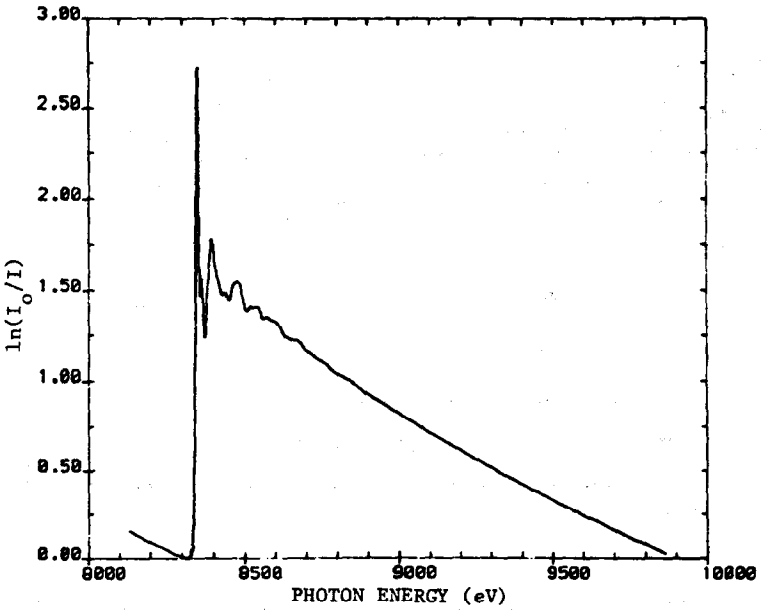

Fig. 2. X-ray absorption spectrum for a plastic-bonded nickel oxide electrode. The electrode composition was 52.6% $Ni(OH)_2$ + 4.2% $Co(OH)_2$ + 24.7% KS-2 graphite + 8.9% carbon fibers + 9.6% Kynar.

$$k = \left\{\frac{2m}{\hbar^2}(E - E_b)\right\}^{1/2} \tag{3}$$

where $E = \hbar\omega$ is the energy of the incident photons, m is the electron mass, and $\hbar$ is Planck's constant divided by 2. If the nickel atoms had no neighbors (*e.g.*, as in an inert gas) then μ would continue to decrease with a smooth E^{-3} dependence beyond the absorption edge. However, neighbor oxygen and nickel atoms in the β-$Ni(OH)_2$, backscatter a small fraction of the outgoing photoelectron wave. Interference between the outgoing wave and the incoming waves from neighboring atoms modulates the photoelectron wave function in the nickel core region, and results in the sinusoidal variation of μ *versus* E. This yields the EXAFS (χ) — the oscillations in the absorption that extend for about 1000 eV above the absorption edge. In energy space, the EXAFS — $\chi(E)$ is defined as

$$\chi(E) = \frac{\mu(E) - \mu_0(E)}{\mu_0(E)} \tag{4}$$

where $\mu(E)$ is the X-ray absorption coefficient and $\mu_0(E)$ is a hypothetical absorption coefficient of the nickel with no surrounding atoms. The $\chi(E)$ function can be converted to photoelectron wave vector (k) space by the relationship in eqn. (2). The physical basis for $\chi(k)$ has been worked out [12] and is given in its simplest form by

$$\chi(k) = \sum_j \frac{N_j}{R_j^2} B_j(k) \exp(-2k^2\sigma_j^2) \exp(-R_j/\lambda(k)) \sin[2kR_j + \phi_j(k)] \quad (5)$$

where N_j refers to the coordination number in a shell of identical atoms, R_j is the respective coordination distance, F_j is the backscattering amplitude of the coordinating atoms, σ_j is the root mean square variation in R_j due to static or thermal disorder (the Debye–Waller factor), $\lambda(k)$ is the mean free path of the photoelectron, and $\phi_j(k)$ is a phase shift due to the photoelectron traversing the distance R_j twice and encountering the potential of the scatter atom once, and that of the absorbing atom twice. The EXAFS is a summation of the effects of different shells of atoms. For a simple case such as a hydrated ion with one coordination shell, the EXAFS is a simple sinusoidal function whose frequency depends on R and the amplitude on the hydration number N. Figure 3 shows the EXAFS for β-$Ni(OH)_2$. It consists of the summation of at least three sinusoidal waves.

This is a rather simplified description of EXAFS. More details are provided in several excellent reviews [13 - 15]. From this description it is evident that the EXAFS contains a lot of information about the coordination of the excited atom.

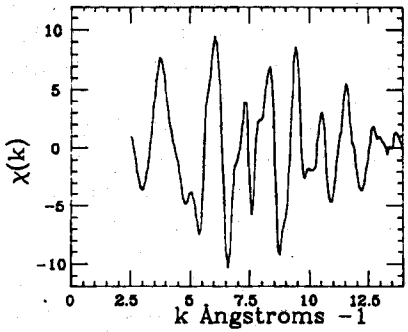

Fig. 3. EXAFS from spectrum in Fig. 2.

Preliminary data analysis — the first Fourier transformation

The aim of data analysis is the determination of the unknown quantities in eqn. (5). The quantities of most interest to chemists are R_j, N_j, and σ_j. The first step is a Fourier transformation of $\chi(k)$. Equation (5) is the superposition of an unknown number of coordination shells. Fourier transformation of $\chi(k)$ yields peaks in r space corresponding to individual shells around the absorbing atom. The Fourier transform is given by

$$\theta_n(r) = \frac{1}{(2\pi)^{1/2}} \int_{k_{min}}^{k_{max}} k^n \chi(k) \exp(2ikr)\, dk \quad (6)$$

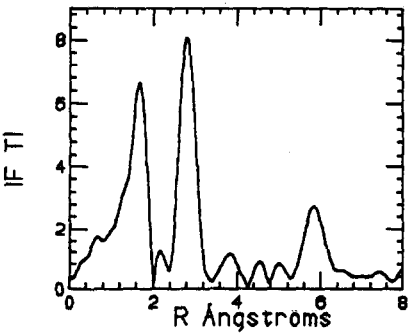

Fig. 4. Fourier transform of data in Fig. 3.

The function $\theta_n(r)$ is called a radial structure function and it contains a series of peaks whose positions, R_j, are related to the coordination distances. Figure 4 is a Fourier transform of the data in Fig. 3. The first peak corresponds to the Ni–O coordination and the second peak to the first Ni–Ni shell in the brucite structure plane. These peaks are shifted to R values that are lower than the actual Ni–O and Ni–Ni distances because of the phase shift $\phi_j(k)$.

Reduction of the raw data in Fig. 2 to the radial structure function in Fig. 4 requires several mathematical manipulations. This includes subtraction of the background, normalization of the EXAFS oscillations and the Fourier transformation. Background subtraction includes a fitting of the pre-edge portion in the spectrum in Figure 2, to within 50 - 70 eV of the edge and extrapolation to the energy region where the EXAFS is present. In this way, the contributions of atoms other than nickel are determined. Fitting is terminated below the edge because of pre-edge features that occur, particularly with transition metals. The EXAFS data are removed from the measured data by subtraction of a cubic spline background. A powerful method for checking whether this is done properly is to examine the derivative of the background and by an iterative technique and a smoothing parameter continue the process until the residual EXAFS oscillations are barely visible in the background derivative. The next step is to normalize the EXAFS by dividing by the height of the absorption edge ($\Delta\mu$) which is usually taken at 50 eV above the absorption edge. To reduce termination errors in the Fourier transform the values of k_{min} and k_{max} are chosen to coincide with nodes in the $\chi(k)$ function. It is a relatively simple process to reach this first stage in the data reduction. Often this suffices, particularly if one wants to only "fingerprint" a material in the same way as diffraction patterns are used. An example is given in Fig. 5 where radial structure functions for cobalt metal foil and pyrolyzed cobalt phthalocyanine on Vulcan XC-72 carbon are shown. The pyrolysis product at 900 °C in argon is obviously cobalt.

Final data analysis — determination of R_j, N_j, and σ_j

After the first Fourier transform is obtained the next step is isolation of the contributions of each shell. In cases like β-$Ni(OH)_2$, where the peaks of

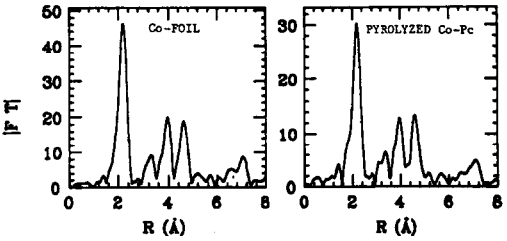

Fig. 5. Radial structure functions for cobalt metal foil and cobalt phthalocyanine on Vulcan XC-72 carbon, after pyrolysis at 900 °C.

the Fourier transform do not overlap (Fig. 4), the contribution from each shell can be isolated by doing an inverse transform of single peaks back to k-space. All other peaks, except the one of interest, are set to zero. Thus, the individual χ_j is isolated. Figure 6 shows an inverse transform of the first peak in Fig. 4. The result is a simple sinusoidal wave of a single shell scatterer.

Once χ_j is isolated, the next step is a separate analysis of the phase ($\Phi(k)$) and amplitude ($A(k)$) functions in eqn. (5). These are, respectively,

$$\Phi(k) = 2kR + \phi(k) \tag{7}$$

and

$$A(k) = \frac{N}{R^2} B(k) \exp(-2k^2\sigma^2) \exp(-R/\lambda(k)) \tag{8}$$

Determination of N, R, and σ depends on knowing $B(k)$, $\phi(k)$ and $\lambda(k)$. The best way of doing this is by comparison with a standard compound (s) of known structure, having identical absorbers and backscatterers to the unknown (u). In this case the standard compound is NiO which has a rock salt structure, an Ni—O distance of (R_s = 2.08 Å), and a coordination number of (N_s = 6). The Debye–Waller factor is given a value $\sigma_s = 0$. So the disorder of β-$Ni(OH)_2$ is determined relative to NiO. The quantities of $B(k)$, $\phi(k)$ and $\lambda(k)$ are assumed to be "transferable" from the standard to the unknown. For NiO, $\phi_u(k_u)$ can be calculated. Then for β-$Ni(OH)_2$, which is the unknown

$$\phi_u(k_u) = \phi_s(k_s)$$

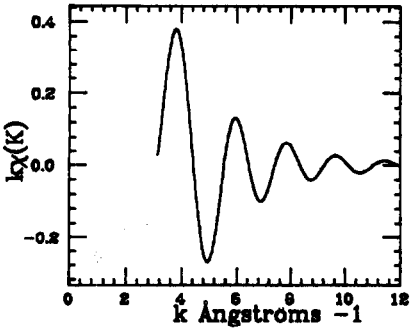

Fig. 6. Inverse transform of the first peak of the Fourier transform in Fig. 4.

After minor corrections for the inner potential (ΔE_0) — differences in absorption edge position for β-$Ni(OH)_2$ and NiO — R_u is calculated as 2.067 Å from

$$R_u = [\Phi(k) - \phi_s(k_s)]/2k$$

This is the Ni—O distance in β-$Ni(OH)_2$. Thus, phase analysis yields actual bond lengths which are somewhat higher than R_j in the radial structure function (Fig. 4).

The value of R_u is then used to do amplitude analyses for the determination of N_u and σ_u. Since σ_u is in a k-dependent term it can be separated from N_u by a simple ratio method involving the logarithms of the ratio of the single shell amplitudes of the unknown and the standard

$$\ln \frac{A_u(k)}{A_s(k)} = \ln \frac{N_u R_s^2}{N_s R_u^2} - \frac{2(R_u - R_s)}{\lambda(k)} - 2k^2(\sigma_u^2 - \sigma_s^2)$$

The k dependence of λ can be neglected, so a plot of $\ln[A_u(k)/A_s(k)]$ *versus* k^2 yields a straight line of intercept

$$\ln \frac{N_u R_s^2}{N_s R_u^2}$$

and slope

$$2(\sigma_u^2 - \sigma_s^2) = 2\Delta\sigma^2$$

Thus, N_u, R_u, and $\Delta\sigma^2$ can be determined. The term $\Delta\sigma^2$ gives the relative disorder for Ni—O in β-$Ni(OH)_2$. The respective values for N_u, R_u, and $\Delta\sigma^2$ are 5.96, 2.067 Å and −0.001 24. Data analysis can be done using theoretical values of the phase and amplitude functions [16].

This data analysis is relatively simple, since the first two shells are well separated and are of widely different atomic numbers (Z). The situation is much more complicated when there are overlapping shells of similar Z value. Examples of these are reported in the literature [17]. A recent book [18] gives further details of data analysis.

X-ray sources for EXAFS studies

The choice of source of X-rays for EXAFS studies is either the bremsstrahlung from a rotating anode X-ray tube or synchrotron radiation from electron or positron storage rings. The EXAFS (Fig. 2) are only about 5% of total absorption. Signal-to-noise ratios (S/N) of greater than 100 are required to determine the EXAFS accurately. Since S/N is proportional to the square root of the X-ray intensity, a high flux of X-ray photons is required. The intensity of a synchrotron source is about 10^4 - 10^6 times higher than from a conventional X-ray tube. This reduces measurement time for a typical EXAFS experiment from a week or more to less than half an hour. Synchrotron radiation also permits studies of dilute samples, including additives and the metallic constituents of metal macrocyclics. Figure 7 shows the EXAFS spectra for the cobalt additive in the nickel oxide electrode of Fig. 2. Even

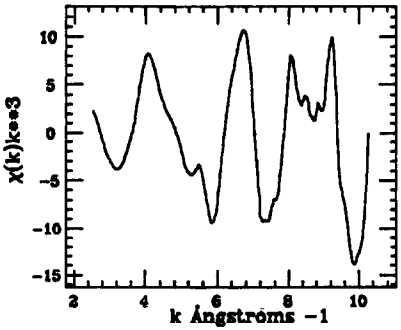

Fig. 7. EXAFS for Co in electrode of Fig. 2.

though the additive is dilute, the spectrum is excellent. However, conventional sources are sometimes convenient. A unit with a rotating anode for electrolyte studies has been described recently [19].

Near edge structure — XANES

The X-ray absorption near edge structure (XANES) portion of the spectrum — within 30 eV of the edge — contains chemical information about the absorbing atom. It depends on the oxidation state of the excited atom, the coordination geometry, and the type of ligands. There is an excellent review of early work in this area [20]. The absorption edge energy shifts linearly with valence state and follows Kunzl's law [21]. XANES is an area of very active experimental and theoretical work. Further theoretical developments will permit its use for a variety of coordination chemistry studies.

Dispersive EXAFS

At present there are two facilities, one in France [22], and the other in Japan [23], for time-resolved EXAFS studies. The technique uses a bent, triangular crystal to focus and disperse the quasi-parallel polychromatic X-ray beam from a synchrotron. The sample of interest is placed in the focal point of the beam. The transmitted beam then diverges towards a position-sensitive detector. The one in France consists of 1024 sensing elements (2500 μm high $\times$ 25 μm wide). This permits acquisition of high quality XANES and EXAFS spectra in times as short as 16 ms. With the advent of detectors with faster response, even shorter times can be achieved. The technique permits *in situ* time-resolved kinetic studies.

Applications of EXAFS and design of experiments

EXAFS is the preferred technique for *in situ* structural studies in electrochemical cells, since both the probe and the signal are X-rays. It is often the only suitable technique for amorphous materials or components of composite structures. It is useful for the study of any element with an atomic number of 16 and above. Once EXAFS is chosen, the important

experimental design aspects are sample preparation, the choice of suitable standards, and the method for detection.

The simplest method of detection is to do transmission EXAFS using the setup shown in Fig. 1. For these experiments, uniformity of the sample is important. If possible, the sample should be chosen to give an absorption of $\Delta\mu x \sim 1.5$ at the edge of interest. Several methods for preparation of uniform solid samples are described in the literature [24 - 26]. Most methods used by battery and fuel cell technologists for preparation of electrodes and separators are useful for preparing samples. One method that the authors have used is a vacuum table technique for casting samples [27, 28]. It is important that the samples be pinhole free and free from cracks. If the elemental composition of a sample is known, the mass of material (M) needed to form a specimen with the desired absorption characteristics can be calculated from the equation

$$M = \frac{A \ln(I_0/I)}{\sum_i f_i(\mu/\rho)_i} \tag{12}$$

where A is the sample area, f_i is the weight fraction of the ith element in the sample, and $(\mu/\rho)_i$ is the mass absorption coefficient of the ith element at the wavelength of interest. Compilations of $(\mu/\rho)_i$ may be found in a report by McMaster [29]. Summary tables are also given in the most recent editions of the *CRC Handbook of Chemistry and Physics* [30]. A value of $\ln(I_0/I) = \Delta\mu x \sim 1.5$ usually gives the best results. However, if a sample contains two or more strong absorbers (*e.g.*, $ZnBr_2$) or is inherently very dilute (*e.g.*, carbon supported platinum catalysts) then lower values of $\Delta\mu x$ may have to be used. However, good data can be obtained with $\Delta\mu x$ values as low as 0.05.

In situ transmission EXAFS of carbon supported platinum electrodes has been done in operating phosphoric acid fuel cells [31] using a slightly modified version of a cell described previously [32]. A cell was designed for *in situ* studies of the charge/discharge processes of plastic bonded nickel oxide electrodes [28]. This is shown in Fig. 8. Equation (12) can be used in the design of cells of this type. Absorbance of cell components in the X-ray path have to be taken into account. It is important that no inhomogeneity, such as current collector wires, be in the path of the beam. Carbon current collectors such as Grafoil are best. Bubbles in electrolyte samples and cells should also be avoided.

For liquid samples such as electrolytes, a sample chamber such as that shown in Fig. 9 is suitable. The chamber thickness can be varied depending on electrolyte concentration. The thickness can be calculated using eqn. (12).

It is important to use good standards which have known excited atom/backscatter coordination. The Fourier transforms for these should have single, well-separated peaks. Thus, ferrocene is a good Fe–C standard, whereas cobaltocene is not a good Co–C standard. The latter has two Co–C distances and overlapping peaks in the Fourier transform. Metal foil standards

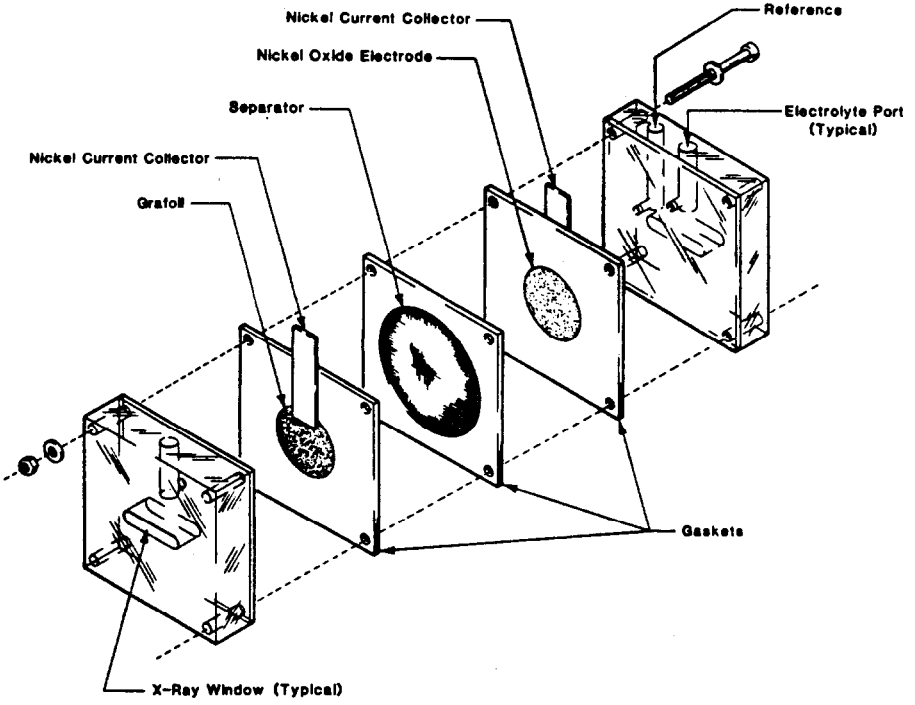

Fig. 8. A cell for *in situ* studies of nickel oxide electrodes.

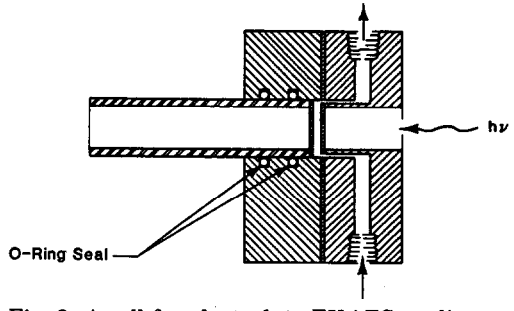

Fig. 9. A cell for electrolyte EXAFS studies.

are usually good for M–M standards, except for b.c.c. metals where the first and second shells overlap.

Apart from transmission measurements, other detection schemes are fluorescence measurements, and electron detection. These methods are reviewed in the literature [14, 33]. Fluorescence methods are very good for working with dilute samples — down to about 100 ppm. Electron detection schemes are useful for investigating processes occurring within a few hundred Angstroms of a surface. With the fluorescence method, homogeneity of the sample is not as critical as in transmission measurements. With electron detection a smooth sample surface appears to be important.

Several synchrotron sources are now available for EXAFS measurements: their locations and characteristics are given in two recent reviews [34, 35]. Several other sources are under construction or are planned [36]. Since the time available at these sources is usually limited, it is very important, particularly in the case of *in situ* measurements, to have electrodes and cells that are functioning properly before doing the EXAFS measurements.

EXAFS studies of battery and fuel cell materials

Even though extensive application of the EXAFS technique is recent, there have been several publications on materials related to batteries and fuel cells. These are briefly reviewed.

Aqueous electrolytes

Early work on the application of EXAFS to aqueous electrolyte studies has been reviewed [13]. The EXAFS technique is unique in that it can sort out ion–ion and ion–water interactions unambiguously. Lagarde *et al.* [37] used EXAFS in a study of $ZnBr_2$ solutions in the concentration range 0.089 - 8.08 M. In going from the lower to the higher concentrations the bromide coordination number increased from 1 to 3.5 and waters of hydration decreased from 7 to 2.5. The Zn–Br bond length was 2.37 Å and the Zn–O bond length was 1.94 Å. Aliotta *et al.* [38] did an EXAFS study of mixed $ZnBr_2$–$CuBr_2$ and mixed $ZnBr_2$–$SrBr_2$ solutions. In both cases it was found that the $CuBr_2$ and $SrBr_2$ acted as bromine donors and that the mean coordination value for bromide ions around zinc increased to four as the bromide to zinc ion ratio increased. Similar increases in the coordination value for bromide ions have been observed on addition of either HBr or $AlBr_3$ to $ZnBr_2$ electrolytes [39]. Other studies of interest to battery researchers are EXAFS investigations of Ni^{2+} ions in concentrated $Ni(NO_3)_2$ solutions [40], Mn^{2+} ions in $MnCl_2$ solutions [41], and the Jahn–Teller complexes of $Cu(H_2O)_6^{2+}$ and $Cr(H_2O)_6^{2+}$ [42].

Polymeric electrolytes

EXAFS of iron in iron neutralized Nafion ionomers has been used to probe ion aggregation in the membrane [43]. This has been done in hydrated and dried membranes.

The poly(ethylene oxide) (PEO) complexes — $RbSCN(PEO)_4$, $RbSCN(PEO)_8$, $RbI(PEO)_4$ and $RbI(PEO)_8$ — have been investigated using EXAFS [44]. These materials are amorphous at room temperature. The results showed that Rb is in well-defined sites of four coordination with ether oxygens, with the actual configuration being anion dependent. In the case of iodide, there are two long and two short Rb–O bonds with the iodide outside the first coordination shell at 3.7 Å. The thiocyanate complexes have a single set of oxygen neighbors and the N atom of the thiocyanate group also appears to be located within the first shell.

Linford *et al.* [45] have done Cu EXAFS on electrolyte from the system

M|CuI + sulfonium iodide|I_2 — perylene

Measurements were made on a freshly prepared electrolyte (a 5.5:1 CuI–4-methyl-1,4-oxathianium iodide adduct) and an electrolyte from a cell after 2000 h of discharge. These results show that the starting electrolyte consists mainly of γ-CuI. After discharge, sulfur appears to be incorporated in the first coordination shell of copper, implying decomposition of the sulfonium cation.

Solid oxide electrolytes

There has been one EXAFS study of yttria-stabilized zirconia over the temperature range −120 to 770 °C [46]. Both Y and Zr EXAFS were obtained in 18 wt.% Y_2O_3-stabilized zirconia. The results indicate that at low temperatures the anion vacancies are preferentially sited closer to the Zr^{4+} ions. This displaces the Zr^{4+} ions from their centrosymmetric sites. Increasing the temperature leads to a random distribution of anion vacancies. Recent results on calcia-stabilized zirconia [47] indicate that the vacancies are also associated with the Zr^{4+} ions. Similar effects have been observed for 40% Y_2O_3 in Bi_2O_3 [48].

In situ studies in cells

In situ EXAFS has been done on the ferrocyanide/ferricyanide system in a thin layer spectroelectrochemical cell [49]. The results show that the Fe–C bond length is 0.03 Å shorter in the ferricyanide than in the ferrocyanide complex.

In situ EXAFS studies have also been done on plastic-bonded, nickel oxide electrodes [26, 50]. During oxidation of $Ni(OH)_2$ to NiOOH there is a contraction along the *a* axis of the $Ni(OH)_2$ brucite structure. The Ni–O distance decreases from 2.04 Å to 1.88 Å. The first Ni–Ni distance also decreases from 3.16 Å to 2.87 Å. On discharge the interatomic distances revert to the original values. During the formation cycles considerable disorder is generated in the $Ni(OH)_2$ structure.

Electrocatalysts

Extensive work has been done using EXAFS to study metal catalysts on non-conductive supports. This work has been reviewed [51]. Good examples of the capabilities of the technique are in the papers of Koningsberger and his co-workers [17, 52 - 54], which includes work on platinum supported on alumina. Other platinum catalysts, including the Adams catalyst, have been investigated [55]. The results indicate that it is a disordered form of α-PtO_2. Recently, EXAFS has been used to study metal–carbon interactions in carbon-supported platinum catalysts in fuel cell electrodes [56]. The data indicate two types of Pt–C interactions.

There is one report on EXAFS studies of pyrolysed cobalt porphyrin catalyst supported on active carbon [57]. The results have been interpreted on the basis that a CoN_4 group is retained in the heat treated catalyst.

Battery materials

EXAFS has been used to study several battery materials such as metal chalcogenides [58] and superionic conductors [59]. Work on other materials of interest to battery research are to be found in several reviews [13 - 15, 34, 60, 61].

XANES studies of battery and fuel cell materials

XANES has been used recently to investigate several battery and fuel cell related materials. These include an investigation of the cerous/ceric redox system [62], the interaction of carbon monoxide with ferric tetrasulfophthalocyanine in alkaline solution [63], a study of vanadium oxides in various oxidation states [64], and an investigation of high temperature corrosion of Fe–Cr alloys [65].

In a recent study [66], XANES spectra were used to detect an SiO_2-like layer at the interface between nickel and an yttria-stabilized zirconia electrolyte. Linford *et al.* [45] also used XANES to identify changes in the copper environment after discharging cells.

An interesting application of XANES is its use as a quantitative technique for the determination of the number of unoccupied d-electron states in platinum catalysts [67].

Synchrotron radiation and fundamental electrochemical studies

The application of synchrotron radiation to fundamental studies of the electrode/electrolyte interface has really only begun. Recent results on the adsorption of iodine on platinum (111) show that the technique can be applied to monolayers [68]. It has also been shown that various fluorescence and electron detection schemes can be used [69]. Electron-yield EXAFS data have been successfully obtained from a nickel surface covered with a thin film of water [70]. Recently, the X-ray standing wave technique has been used to study iodine and copper layers on platinum [71]. Several other synchrotron radiation techniques have been used for the study of chemisorbed atoms and molecules. These have been reviewed [72] and some are applicable to electrochemical systems. Another promising technique for fundamental studies is X-ray topography [73]. Many of these techniques, such as X-ray standing wave and X-ray topography, are old, but synchrotron radiation greatly reduces data acquisition times.

Advantages of EXAFS and future applications

Progress in basic and applied electrochemical research has been hampered because of the lack of a technique for *in situ* studies at a molecular level [74]. The small amount of work so far indicates that synchrotron radiation techniques will change this. The EXAFS technique is versatile in that it is element specific and can be applied to most elements in the periodic table. Furthermore, it can be applied to all states of matter, whether they be solids, liquids, gases, or absorbed monolayers. It is an excellent technique for investigations of dilute systems. Together with XANES it yields both chemical and structural information.

Unlike X-ray diffraction of single crystals, EXAFS is not an *ab initio* structural determination technique. However, many battery active materials, electrolytes, and electrocatalysts cannot be prepared as single crystals. EXAFS is the best technique for studying these amorphous materials. With a careful choice of standards and exhaustive data analysis for phase and amplitude, unknown coordinating atoms can be determined by EXAFS. The relative merits of EXAFS and diffraction have been recently reviewed [75].

From a basic point of view, the greatest impact of these X-ray techniques will be new insights into the electrode/electrolyte interface. It will also attract scientists from other disciplines to electrochemistry. In practical applications, it will permit *in situ* studies of active material and catalyst preparation, including catalyst-support interactions. The investigation of performance limiting and degradation mechanisms can be studied in actual cells at a molecular level. EXAFS is an excellent technique for investigating disordered materials and materials with defects. An example of the latter are transformation-toughened ceramics. With the advent of more synchrotron sources [34 - 36] and the development of more simplified data analysis packages the technique will find widespread use.

Acknowledgements

The data reported in the Figures in this paper were obtained at Beam Line X-11 of the National Synchrotron Light Source at Brookhaven National Laboratory. The authors thank the Department of Energy, Division of Materials Sciences, for operating funds for Beam Line X-11, under Contract DE-AC05-80ER10742.

List of Symbols

A Sample area
$A(k)$ Amplitude of EXAFS as a function of k
$A_s(k)$ Amplitude of EXAFS for standard excited atom–backscatterer combination

$A_u(k)$ Amplitude of EXAFS for unknown compound
$A_j(k)$ Amplitude of EXAFS for a particular coordination shell j of the same type of atoms at a distance R_j from the excited atom
$B(k)$ The backscattering amplitude of neighbor atoms around the excited atom; the subscripts s, u and j have the same meaning as for $A(k)$
E Energy of the X-ray photon
E_b Binding energy of a core electron in the absorber atom
f_i Weight fraction of an element i in a sample
I Intensity of transmitted X-ray beam
I_0 Intensity of incident X-ray beam
k Wave vector of ejected photoelectron
m Mass of the electron
N_j Coordination number for a single shell, j, of backscatterers; the subscripts s and u have the same meaning as for $A(k)$
R_j The distance between an absorber atom and a single shell, j, of backscatterers; the subscripts s and u have the same meaning as for $A(k)$
x Sample thickness
$\hbar$ Planck's constant divided by 2
$\theta_n(r)$ Fourier transfer of the EXAFS, called the radial structure function
λ Wavelength of the photoelectron
$\lambda(k)$ Mean free path length of the photoelectron
μ X-ray absorption coefficient of a sample
$\mu(E)$ X-ray absorption coefficient of an absorber as a function of photon energy
$\mu_0(E)$ X-ray absorption coefficient of an absorber without any backscatterers
$(\mu/\rho)_i$ Mass absorption coefficient of the element i
σ_j Deviation in R_j caused by static and thermal disorder of the backscatterer j
$\Delta\sigma_j^2$ Debye–Waller factor — deviation of σ^2 with respect to some standard
$\phi_j(k)$ The phase shift due to a single shell of backscatterers j; the subscripts s and u have the same meaning as for $A(k)$
Φ The argument of the sin term in the EXAFS — eqn. (5)
χ The EXAFS
ω Radial frequency of X-ray photon

References

1 R. V. Biagetti and M. C. Weeks, *Bell. Syst. Tech. J., 49* (1970) 1305.
2 R. J. Brodd, A. Kozawa and K. V. Kordesch, *J. Electrochem. Soc., 125* (1978) 271c.
3 D. F. Pickett, U. D. Martin, J. W. Logsdon and J. F. Leonard, *Proc. 27th Power Sources Symp.*, PSC Publications, Red Bank, NJ, 1976, pp. 120 - 123.
4 P. Ehrburger, D. P. Mahajan and P. L. Walker, Jr., *J. Catal., 43* (1976) 61.
5 J. McBreen and E. Gannon, *J. Electrochem. Soc., 130* (1983) 1667.

6 R. F. Gahn, N. H. Hagedorn and J. S. Long, *Proc. 18th Intersoc. Energy Conv. Eng. Conf.*, Vol. 4, 1983, pp. 1647 - 1652; *Chem. Abstr. 99:161425b.*
7 L. M. Peter, W. Durr, P. Bindra and H. Gerischer, *J. Electroanal. Chem., 71* (1976) 31.
8 R. Barnard, C. F. Randell and F. L. Tye, *J. Appl. Electrochem., 10* (1980) 109.
9 J. P. Brenet and S. Ghosh, *Electrochim. Acta, 7* (1962) 449.
10 K. Wiesener, *Electrochim. Acta, 31* (1986) 1073.
11 J. E. Enderby and G. W. Neilson, *Rep. Prog. Phys., 44* (1981) 593.
12 D. E. Sayers, E. A. Stern and F. W. Lytle, *Adv. X-ray Anal., 13* (1970) 248.
13 P. A. Lee, P. H. Citrin, P. Eisenberger and B. M. Kincaid, *Rev. Mod. Phys., 53* (1981) 769.
14 E. A. Stern and S. M. Heald, in E. E. Koch (ed.), *Handbook on Synchrotron Radiation*, Vol. 1, North-Holland, Amsterdam, 1983, Ch. 10, pp. 955 - 1014.
15 T. M. Hayes and J. B. Boyce, *Solid State Phys., 37* (1982) 173.
16 B. K. Teo and P. A. Lee, *J. Am. Chem. Soc., 101* (1979) 2815.
17 J. B. A. D. Van Zon, D. C. Koningsberger, H. F. J. Van't Blick and D. E. Sayers, *J. Chem. Phys., 82* (1985) 5742.
18 B. K. Teo, *EXAFS Basic Principles and Data Analysis*, Springer, Berlin, 1986.
19 P. Dreier and P. Rabe, *Rev. Sci. Instrum., 57* (1986) 214.
20 U. C. Srivastava and H. L. Nigam, *Coord. Chem. Rev., 9* (1972) 275.
21 V. Kunzl, *Trav. Chim. Czech., 4* (1932) 213.
22 A. M. Flank, A. Fontaine, A. Jucha, M. Lemonier, D. Raoux and C. Williams, *Nucl. Instr. Methods, Phys. Res., 208* (1983) 651.
23 R. P. Phizackerley, Z. V. Rek, G. B. Stephenson, S. D. Couradson, K. O. Hodgson, T. Matsushita and M. Onyanayi, *J. Appl. Crystallogr., 16* (1983) 220.
24 E. D. Eanes, J. L. Costa, A. MacKenzie and W. K. Warburton, *Rev. Sci. Instrum., 51* (1980) 1579.
25 K.-Q. Lu and E. A. Stern, *Nucl. Instrum. Methods Phys. Res., 212* (1983) 475.
26 J. Wong, *Nucl. Instrum. Methods, Phys. Res., A238* (1985) 554.
27 J. McBreen, *U.S. Pat. 4,000,005*, Dec. 28, 1976.
28 J. McBreen, W. E. O'Grady, K. I. Pandya, R. W. Hoffman and D. E. Sayers, *Langmuir, 3* (1987) 428.
29 W. H. McMaster, N. Kerr Del Grande, J. H. Mallet and J. H. Hubbell, *Rep. UCRL - 50174*, Lawrence Radiation Lab., Univ. California, Livermore.
30 R. C. Weast and M. J. Astle (eds.), *CRC Handbook of Chemistry and Physics*, CRC Press, Boca Raton, FL, 1981, pp. E-139 - 143.
31 W. E. O'Grady, D. E. Sayers, J. I. Budnick and G. H. Hayes, *Ext. Abstr., No. 639, Proc. Electrochem. Soc.*, Vol. 85-1, 1985, pp. 895 - 896.
32 H. Olender, J. McBreen, W. E. O'Grady, S. Srinivasan and K. V. Kordesch, *J. Electrochem. Soc., 129* (1982) 135.
33 S. M. Heald, in D. C. Koningsberger and R. Prins (eds.), *Application Techniques of EXAFS, SEXAFS and XANES*, Wiley, New York, 1987.
34 J. Wong, *Mater. Sci. Eng., 80* (1986) 107.
35 C. R. A. Catlow and E. N. Greaves, *Chem. Brit., 22* (1986) 805.
36 A. L. Robinson, *Science, 235* (1987) 841.
37 P. Lagarde, A. Fontaine, D. Raoux, A. Sadoc and P. Migliardo, *J. Chem. Phys., 72* (1980) 3061.
38 F. Aliotte, G. Galli, G. Maisano, P. Migliardo, C. Vasi and F. Wanderlingh, *Nuovo Cimento, 2D* (1983) 103.
39 J. McBreen, W. E. O'Grady, D. Sayers and C. Y. Yang, *Ext. Abstr. No. 574, Proc. Electrochem. Soc.*, Vol. 86-1, 1986, pp. 834 - 835.
40 G. Licheri, G. Pashcina, G. Piccaluga, G. Pinna and G. Vlaic, *Chem. Phys. Lett., 82* (1981) 384.
41 B. Beagley, B. Gahan, G. N. Greaves, C. A. McAuliffe and E. W. White, *J. Chem. Soc., Chem. Commun.*, 1804 (1985).
42 T. K. Sham, J. B. Hastings and M. L. Pearlman, *Chem. Phys. Lett., 83* (1981) 391.

43 H. K. Pan, D. J. Yarusso, G. S. Knapp, M. Pineri, A. Meagher, J. M. D. Coey and S. L. Cooper, *J. Chem. Phys., 79* (1983) 4736.
44 C. R. A. Catlow, A. V. Chadwick, G. N. Greaves, L. M. Moroney and M. R. Worboys, *Solid State Ionics, 9* (1983) 1107.
45 R. G. Linford, P. G. Hall, C. Johnson and S. S. Hasnian, *Solid State Ionics, 14* (1984) 199.
46 C. R. A. Catlow, A. V. Chadwick G. N. Greaves and L. M. Moroney, *J. Am. Ceram. Soc., 69* (1986) 272.
47 L. M. Moroney and D. E. Sayers, *J. Phys., 47* (1986) C8-725.
48 P. D. Battle, C. R. A. Catlow, A. V. Chadwick, G. N. Greaves and L. M. Moroney, *J. Phys., 47* (1986) C8-669.
49 D. A. Smith, R. C. Elder and W. R. Heineman, *Anal. Chem., 57* (1985) 2361.
50 J. McBreen, W. E. O'Grady and D. E. Sayers, *Ext. Abstr. No. 105, Proc. Electrochem. Soc.*, Vol. 86-2, 1986, pp. 151 - 152.
51 R. W. Joyner and P. Meehan *Vacuum, 33* (1983) 691.
52 D. C. Koningsberger, J. B. A. D. van Zon, H. F. J. van't Blik, G. J. Visser, R. Prins, A. N. Mansour, D. E. Sayers, D. R. Short and J. R. Katzer, *J. Phys. Chem., 89* (1985) 4075.
53 D. C. Koningsberger and D. E. Sayers, *Solid State Ionics, 16* (1985) 23.
54 F. B. M. Duivenoorden, D. C. Koningsberger, Y. S. Uh and B. C. Gates, *J. Am. Chem. Soc., 108* (1986) 6254.
55 A. N. Mansour, D. E. Sayers, J. W. Cook, Jr., D. R. Short, R. D. Shannon and J. R. Katzer, *J. Phys. Chem., 88* (1984) 1778.
56 W. E. O'Grady and D. C. Koningsberger, *J. Chem. Phys.* (to be published).
57 R. W. Joyner, J. A. R. van Veen and W. M. H. Sachtler, *J. Chem. Soc., Faraday Trans. I, 78* (1982) 1021.
58 S. P. Cramer, K. S. Liang, A. J. Jacobsen, C. H. Chang and R. R. Chianelli, *Inorg. Chem., 23* (1984) 1215.
59 T. M. Hayes, J. B. Boyce and J. L. Beeky, *J. Phys., 11* (1978) 2931.
60 D. R. Sandstrom and F. W. Lytle, *Annu. Rev. Phys. Chem., 30* (1979) 215.
61 B. Lengeler, *Z. Phys. B, 61* (1985) 421.
62 T. K. Sham, *J. Chem. Phys., 79* (1983) 1116.
63 C. A. Linkous, W. E. O'Grady, D. E. Sayers and C. Y., Yang, *Inorg. Chem., 25* (1986) 3761.
64 J. Wong, F. W. Lytle, R. P. Messner and D. H. Maylotte, *Phys. Rev. B, 30* (1984) 5596.
65 G. G. Long, J. Druger and D. Tanaka, *J. Electrochem. Soc., 134* (1987) 264.
66 D. Gozzi, M. Tomellini, A. Bianconi and M. Fanfoni, *J. Electroanal. Chem., 198* (1986) 53.
67 A. N. Mansour, J. W. Cook and D. E. Sayers, *J. Phys. Chem., 88* (1984) 2330.
68 J. G. Gordon II, O. R. Melroy, G. L. Borges, D. L. Reisner, H. D. Abruna, P. Chandrasekhar and L. Blum, *J. Electroanal. Chem., 210* (1986) 311.
69 M. E. Kordesch and R. W. Hoffman, *Nucl. Instr. Methods Phys. Res., 222* (1984) 347.
70 K. I. Pandya, K. Yang, R. W. Hoffman, W. E. O'Grady and D. E. Sayers, *J. Phys., 47* (1986) C8-159.
71 M. J. Bedzyk, D. Bilderback, J. White, H. D. Abruna and M. G. Bommarito, *J. Phys. Chem., 90* (1986) 4926.
72 J. Stohr, *Z. Phys. B, 61* (1985) 439.
73 W. Graeff, *Z. Phys. B, 61* (1985) 469.
74 E. Yeager, *Surf. Sci., 101* (1980) 1.
75 D. Raoux, *Z. Phys. B, 61* (1985) 397.